Sense codon-misassociated eRF1 elicits widespread ribosome stalling and induction of quality control

Peixun Han[1], Mari Mito[1], Takuhiro Ito[2], and Shintaro Iwasaki[1,2,4,†]

[1]RNA Systems Biochemistry Laboratory, RIKEN Cluster for Pioneering Research, Wako, Saitama 351-0198, Japan

[2]Laboratory for Translation Structural Biology, RIKEN Center for Biosystems Dynamics Research, Tsurumi-ku, Yokohama 230-0045, Japan

[3]Department of Computational Biology and Medical Sciences, Graduate School of Frontier Sciences, The University of Tokyo, Kashiwa, Chiba 277-8561, Japan

[4]Lead contact

[†]Correspondence: shintaro.iwasaki@riken.jp (S.I.)

Abstract

Ribosome-associated quality control (RQC) is a surveillance system for aberrant translation that senses ribosome collisions. Although the molecular mechanism has been extensively studied, the endogenous targets of RQC in human cells are poorly understood. Here, beginning with a study of the codon specificity of the eukaryotic translation termination factor eRF1, we show that transient binding of eRF1 to the UUA sense codon leads to ribosome collision and provides a source of RQC substrates in humans. eRF1-selective Monosome-Seq and Disome-Seq revealed that eRF1 was recruited not only to stop codons but also to subcognate sense codons, including the UUA codon. The eRF1 on UUA codons delays translation elongation but does not trigger the termination reaction. Remarkably, Disome-Seq with the depletion of ASCC3 and 4EHP, key factors in RQC, showed that ribosomes stalled at UUA codons constitute a predominant subpopulation rescued by RQC. Failure to resolve ribosome collisions by RQC triggers p38 phosphorylation and expression of the stress-induced transcription factor ATF3. This study highlights the impact of sense codon misrecognition by the termination factor on translation homeostasis in human cells.

Introduction

Protein translation is subject to surveillance systems to maintain cellular homeostasis [1–4]. Extensive efforts over the last decade have revealed the surveillance pathway associated with ribosome collision [1–4]. In typical growing human cells, ribosomes are sparsely located every 200–400 nt in mRNAs [5–10]. However, once the ribosome encounters obstacles to its traversal along open reading frames (ORFs), it may pause in the middle of nascent chain elongation. Consequently, trailing ribosomes queue to the leading ribosomes to generate colliding di-ribosomes or disomes. By recruiting specific factors, disomes function as platforms to induce downstream signaling [1–4].

Ribosome-associated quality control (RQC) is one such mechanism. In this pathway, a disome recruits the E3 ligase ZNF598 (Hel2 in yeast), which recognizes the 40S–40S interface between two collided ribosomes [11–18]. This ubiquitin modification allows the helicase ASCC3 (Slh1 in yeast) to split the leading ribosome in an ATP-dependent manner, permitting the trailing ribosome to resume elongation [13,17–21]. Simultaneously, colliding ribosomes trigger the repression of translation initiation through the scaffold protein GIGYF2 and the initiation repression factor 4EHP (also known as eIF4E2) [22–26]. The temporal reduction in ribosome loading onto the transcript could prevent further ribosome collision. The nascent peptide located on the split 60S is degraded by the E3 ligase Listerin (Ltn1 in yeast) and NEMF (Rqt2 in yeast), with the aid of Ala-Thr tailing at the C-terminus of the nascent peptide (CAT-tailing; see citations reviewed in [1–4]).

The discovery of this mechanism was based on reporter systems, which induce ribosome stalling [11,27]. The endogenous target sites of RQC were subsequently identified, including *SDD1* mRNA in yeasts [17], *XBP1u* mRNA in humans [28], and *C-I30* mRNA in

flies [29]. More broadly, poly-Lys motifs are natural substrates for yeast RQC [30], whose demand increases with age [31]. Additionally, yeast RQC manages chemically damaged mRNAs [32]. However, our knowledge of the endogenous mRNAs targeted by RQC still needs to be completed, especially in human cells.

Recent studies have shown that stop codons are generally a disome-rich position [28,30,33]. Translation termination is mediated by eRF1 in eukaryotes. Unlike bacteria, which have two termination factors (RF1 and RF2), eRF1 is responsible for recognizing all three stop codon species (UAA, UAG, and UGA) [34]. By forming a complex with the GTPase eRF3, eRF1 releases peptides from P-site tRNAs. While structural studies [35–37] and single-molecule analysis [38] have revealed that eRF1 recognition of stop codons is highly specific and efficient, potential binding to subcognate sense codons has been suggested [39,40]. However, a genome-wide survey of eRF1-ribosome associations remains unaccomplished.

We reconciled these two distinct translation events; unexpectedly, our investigation of eRF1 codon recognition revealed endogenous RQC substrates in human cells. eRF1-selective Monosome-Seq and Disome-Seq showed that eRF1 binds to only stop codons but also subcognate sequences, including UUA codons. This tentative UUA codon binding does not achieve peptidyl-tRNA cleavage but leads to ribosome stalling and collision. Congruently, disomes predominantly accumulate on UUA codons upon RQC factor depletion, suggesting that the association of eRF1 with a UUA sense codon serves as a major substrate for RQC in cells. Our reporter assay confirmed this model. We also showed that an absence of RQC factors induces the ribotoxic stress response (RSR) and ATF3 expression for transcriptome remodeling. Our study reveals natural RQC targets and the importance of this surveillance for maintaining cellular homeostasis.

Results and discussion

eRF1 binds to UUA sense codons and pauses ribosomes

To determine the codon recognition diversity of eRF1, we isolated ribosomes associated with eRF1 and then subjected them to ribosome profiling (*i.e.*, selective Monosome-Seq) (Figure 1A) [41,42]. For this purpose, we generated a stable HEK293 cell line that expressed streptavidin-binding peptide (SBP)-tagged eRF1 in a tetracycline-inducible manner (Figure S1A). Simultaneous RNase treatment and immunoprecipitation (IP) allowed us to enrich ribosomes directly bound to eRF1 and exclude those bound through mRNAs in the form of polysomes (Figure 1A). Notably, to enable eRF1-baited pulldown of ribosomes and footprints, we used micrococcal nuclease (MNase), which maintains ribosome integrity [43], rather than RNase I, a standard RNase used for ribosome footprinting [44–47]. Consistent with a report that eRF1 in the ribosomal A site protects footprints from 3′ end trimming by RNase [48], eRF1-selective Monosome-Seq excluded short (~21-23 nt) footprints (Figure S1B).

Compared with those from the input libraries, ribosome footprints from the eRF1-IP libraries were relatively accumulated at stop codons (Figures 1B-C and S1C). However, eRF1 binding to mRNAs was not exclusive to stop codons; to our surprise, eRF1 was also associated with ribosomes at a subset of sense codons (Figures 1B-C and S1C). In particular, these sense codons included those that can be considered near-cognate stop codons such as UGU, UGG, UGC, and UUA (Figures 1C and S1C), suggesting the possibility of misrecognition of the subcognate codons by eRF1.

Given that eRF1-mediated sense codon misrecognition is unwelcome, we reasoned that this phenomenon may cause ribosome stalling and thus lead to a collision with trailing ribosomes. To test this possibility, we applied disome profiling [28,30,33,49,50] to

the complexes isolated with SBP-eRF1 (*i.e.*, selective Disome-Seq) (Figures 1A and S1D). As observed in eRF1-selective Monosome-Seq experiments, a longer population of disome footprints was enriched in eRF1-selective Disome-Seq (Figure S1D). As in monosome footprints (Figure 1C), disomes containing eRF1 were relatively enriched in stop codons (Figures 1D and S1E), as the leading ribosomes are stalled on stop codons. Notably, we observed even stronger enrichment of disome footprints on subcognate UUA codons than on cognate stop codons (Figure 1D and 1E).

Considering that UUA may be a part of a UAA or UAG stop codon via a +1 frameshift, we investigated the possibility that disomes formed on UUA codons could stem from stop codons translated along a +1 frame by frameshifting. However, the occupancy of eRF1-associated disomes on UUA-A and UUA-G was not greater than that on UUA-U (Figure S1F). Therefore, the stalling of eRF1-associated ribosomes on UUA is unlikely to be attributed to out-of-frame stop codons.

These data indicate that eRF1 recruitment to a UUA codon causes ribosome collision.

UUA-misrecognizing eRF1 does not complete the translation

Next, we investigated whether the association of eRF1 with a sense codon leads to a termination reaction or peptidyl-tRNA cleavage. After the termination reaction by eRF1, ABCE1 dissociates 60S subunits from 80S ribosomes on the stop codons for recycling. Since ABCE1 functions only after peptidyl-tRNA cleavage, ribosome accumulation on stop codons by ABCE1 depletion ensures that proper translation termination reactions are induced at those positions [51–55]. Here, we used Disome-Seq because of its high sensitivity for detecting ribosome stalling. Notably, the application of Ribo-FilterOut [10] techniques

enabled greater recovery of usable reads than our previous approach involving Cas9-mediated removal of specific sequences (DASH: depletion of abundant sequences by hybridization) [28,46] (Figure S2A) because of effective removal of contaminated rRNA fragments. Additionally, we utilized the Thor (T7 high-resolution original RNA) technique, which is based on T7 polymerase-mediated RNA amplification for low-input RNA [56]. These modifications allowed stable library preparation for a limited number of disome footprints.

Indeed, siRNA-mediated knockdown of ABCE1 (Figure S2B-D) increased the disomes with unrecycled ribosomes on stop codons (Figure 1F), as shown by the results of Monosome-Seq in earlier studies [51–55]. Moreover, we observed an additional queue of collided ribosomes 10-codon (1 ribosome size) upstream from the stop codons (Figure 1F), indicating trisome formation [28]. We found that UUA codons, which are associated with eRF1-mediated ribosome stalling (Figure 1E), generally led to disome formation (Figure 1G). However, it was not affected by ABCE1 depletion without the formation of trailing trisomes (Figure 1G), suggesting that ribosomes stalled on UUA codons do not result in termination reactions and subsequent recycling.

The same conclusion was supported by selective Monosome/Disome-Seq for peptidyl-tRNA cleavage-deficient eRF1. Conversion of the GGQ motif to AAQ allows a conformational change in eRF1, which is associated with GTP hydrolysis by eRF3, but it cannot induce the cleavage of peptidyl-tRNA [35,37,57,58]. Ultimately, eRF1 AAQ may accumulate dead-end complexes of ribosomes after the accommodation of the middle (M) domain of eRF1 into the peptidyl transferase center (PTC) [35,37] (Figure S3A). As expected, the AAQ eRF1 mutant was associated with disomes in which the leading ribosomes are located on canonical stop codons (Figure 1H and Figure S3B-C). However, compared

with wild-type (WT) eRF1, the association of AAQ eRF1 with disomes on UUA codons was attenuated (Figure 1D and 1H), indicating that eRF1 on the UUA codon does not proceed to the PTC accommodation step.

Thus, taking these data together, we conclude that eRF1 may bind tentatively to ribosomes on UUA codons but does not trigger the hydrolysis of peptidyl-tRNA.

eRF1 delays ribosome traversal at UUA codons

To understand the structural basis of eRF1's misbinding to the UUA codon, we revisited the published 80S•eRF1•eRF3 complex recognizing the UGA stop codon and the downstream G nucleotide[37] and assessed nucleotide interchangeability (Figure S3D). In the structure, the 3-NH of U+1 is hydrogen bonded to the oxygen of the phosphate group of G+4. On the other hand, the 2′-OH of U+1 forms a hydrogen bond with the N7 of A+3, permitting the same interaction when the +3 position is G. The N7 of G+2 (or A+2) is recognized through Mg^{2+}; U+2 may also be allowed at this position. However, the 4-NH_2 of C+2 is likely to interfere with Mg^{2+}. Since at least one 6-NH_2 of A+2 or A+3 needs to be recognized by Glu55 of eRF1[35], UUA is compatible, but UUG is not (Figure S3D).

Given these findings, we reasoned that misrecognition by eRF1 of UUA codons may compete with Leu-$tRNA^{Leu}_{UAA}$ and delay protein synthesis. To test this possibility, we conducted an *in vitro* translation assay with rabbit reticulocyte lysate (RRL) utilizing nanoluciferase (Nluc) as a reporter. We prepared two types of reporter mRNAs: one predominantly uses CUG codons, the most frequent Leu codon in the human genome, and the other uses UUA codons. In total, 11 out of the 16 leucine codons in Nluc were substituted with CUG or UUA (Figure 2A, top: 11× CUG and 11× UUA). Upon the addition of recombinant eRF1-eRF3 to the reaction mixture, we observed decreased

protein synthesis from the 11× UUA reporter but not from the 11× CUG reporter (Figure 2A, bottom).

Additionally, we observed similar molecular phenotypes in the cells. We compared the results of standard Monosome-Seq and Disome-Seq with or without additional SBP-eRF1 expression and found that ribosomes are stalled on UUA codons by excessive eRF1 (Figure 2B).

Moreover, we observed that eRF1-binding to UUA codons is a stoichiometric event. Stop codon recognition by eRF1 pulls the 4th position nucleotide into the ribosome A site[35], allowing the 1-nt longer ribosome footprints[59]. Consistent with these reports, we observed 30-nt footprints, 1-nt longer than major 29-nt footprints, at stop codons (Figure 2C). We found that footprints at the UUA codons showed an increased population of 30-nt footprints (Figure 2C). These data suggested that a substantial fraction of ribosomes on UUA were associated with eRF1.

These data indicate that the misrecognition of UUA by eRF1 leads to a delay in elongation and subsequent ribosome collision.

The RQC system rescues ribosome collision formed on UUA codons

The ribosome collision induced by sense codon-misrecognizing eRF1 led us to investigate the involvement of RQC in this rescue. For this purpose, we surveyed disomes accumulated due to the loss of RQC. Recent findings have demonstrated that the leading ribosome in a ribosome collision can be split by the ATP-dependent helicase ASCC3 [13,17–21] (Figure 3A). Moreover, colliding ribosomes can also act as platforms to repress translation initiation, preventing further ribosome collision, through the recruitment of 4EHP, a cap-binding protein [22–26] (Figure 3A). Using siRNA-mediated gene knockdown,

we suppressed both mechanisms to maximize the generation of disomes that are subjected to RQC (Figure S2B-D).

Remarkably, upon ASCC3-4EHP double depletion, we observed a pile-up of disomes where leading ribosomes were at UUA codons (Figure 3B). These collisions at UUA codons subsequently led to queued trisomes (Figure 3C). On the other hand, a single knockdown of each factor did not affect ribosome collision at UUA codons (Figure 3D), suggesting that multiple regulatory points in RQC may synergistically function to suppress/resolve ribosome collision.

In addition to the general trends involving UUA codons, our data revealed ribosome collision sites that are rescued by RQC. In the ASCC3-4EHP double-depleted cells, we identified 1973 disome peak sites (see Methods), three-quarters of which were already present in the control knockdown samples (Figure 3E). The remaining one-quarter (470 sites) represented ribosome collision sites that emerged upon the loss of ASCC3-4EHP double depletion or RQC targeting sites. Again, the newly generated disome pause sites were found at UUA codons at a statistically significant level (Figure 3E), which is consistent with the global increase in high disome occupancy on UUA codons (Figure 3B). These loci were exemplified by UUA codons in *PNRC1* and *CCT7* mRNAs (Figure 3F).

Notably, unlike those in yeast [30,31], the poly-Lys motifs found in endogenous mRNAs were not subjected to RQC under our conditions. Although the Lys-rich motif of *MTDH* mRNA is known to induce ribosome stalling [28,60], ribosome collision at this motif was not further strengthened by ASCC3-4EHP double depletion (Figure S4A). More broadly, the RQC defect had limited effects on disome occupancy at Lys-Lys motifs (P-A sites) (Figure S4B). This observation was congruent with an earlier report that the

human RQC system recognizes longer Lys-AAA repeats than the yeast system does [13]. The human genome tends to evade such long repeats.

Given the correspondence of disome formation at UUA codons, we hypothesized that ribosome collision induced by eRF1 misrecognition of UUA may generate substrates for RQC in cells. To test this scenario, we utilized an 11× UUA Nluc reporter (Figure 2A) to monitor the impact of ribosome stalling at UUA codons in cells. We observed that ASCC3-4EHP double knockdown reduced protein synthesis in the 11× UUA Nluc reporter (Figure 3G) because of ribosome stalling and collision at UUA codons. Strikingly, this repression was not detected when the expression of eRF1 was reduced (Figures 3G and S2E). These data demonstrate that eRF1 recruitment to UUA codons is a general cause of ribosome stalling that can be rescued by the RQC mechanism.

Unresolved ribosome collisions at UUA codons trigger a ribotoxic stress response and ATF3 expression

Next, we investigated the cellular responses triggered when colliding ribosomes were left unresolved at UUA codons. In addition to the RQC pathway, other responses, including the ribotoxic stress response (RSR) mediated by MAP3K ZAKα activation, have been highlighted in recent studies [61–66]. In the RSR, ZAKα activates downstream signaling pathways including p38 activation [61–67]. We reasoned that the accumulation of disomes upon depletion of the RQC factors ASCC3 and 4EHP may trigger crosstalk with the RSR. Consistent with this scenario, we observed the phosphorylation of p38, a hallmark of p38 activation (Figure 4A).

A recent study showed that RSR activation induces transcriptome remodeling through the accumulation of the stress-inducible transcription factor ATF3 [68]. We found

that ATF3 expression was increased upon the double knockdown of ASCC3 and 4EHP (Figure 4A). The accumulation of the ATF3 protein was attributed to the upregulation of its mRNA abundance (Figure 4B), along with large-scale alterations in the cellular transcriptome. The double depletion of ASCC3 and 4EHP induced the expression of direct targets of ATF3 (such as GDF15, DDIT3, and CCL5) [69] (Figure 4C). These data suggest that unresolved disomes activate RSR to induce cellular stress response pathways.

Conclusion

Our work reveals unexpected impacts of the association of eRF1 with the UUA sense codon for translation quality control (Figure 4D). Our results show that eRF1 may transiently associate with widespread sense codons before full accommodation by GTP hydrolysis of eRF3 in cells. This phenomenon may allow for initial selection for faithful translation termination and provide an opportunity for the reduction in premature completion of protein synthesis at unintended codon sequences. A similar fidelity check mechanism was found in the translation elongation process [70]. Subcognate and rare UUA codons in the human genome may extend the dwell time of eRF1-eRF3 during initial selection and ultimately slow ribosome traversal by competing with cognate tRNAs. This process is a double-edged sword; while it ensures the accuracy of translation termination, it also causes unwelcome ribosome collision. RQC may resolve this conflict and provide resilience in cellular proteostasis.

Acknowledgments

We are grateful to all the members of the Iwasaki laboratory for their constructive discussions and technical help. Computation was supported by the HOKUSAI SailingShip supercomputer facility at RIKEN. We are grateful to the Support Unit for Bio-Material Analysis, RIKEN CBS Research Resources Division, for Sanger sequencing. We also thank Dr. Nicholas T. Ingolia for sharing plasmids. This work was supported by the Ministry of Education, Culture, Sports, Science and Technology (MEXT) (JP20H05784 and JP24H02307 to S.I.; JP21H05281 to T.I.), the Japan Agency for Medical Research and Development (AMED) (JP20gm1410001 to S.I. and T.I.), the Japan Society for the Promotion of Science (JSPS) (JP23H02415 and JP23H00095 to S.I.; JP22J13110 and JP22KJ0894 to P.H.), and RIKEN (Pioneering Project to S.I. and T.I.). P.H. was the JSPS Research Fellow (DC2/PD).

Author contributions

Conceptualization: P.H. and S.I.;

Methodology: P.H., M.M., and S.I.;

Formal analysis: P.H.;

Investigation: P.H. and M.M.;

Resources: T.I.;

Writing – Original Draft: P.H. and S.I.;

Writing – Review & Editing: P.H., M.M., T.I., and S.I.;

Visualization: P.H. and S.I.;

Supervision: T.I. and S.I.;

Project administration: S.I.;

Funding Acquisition: P.H., T.I., and S.I.

Declaration of interests

S.I. is a member of the *Scientific Reports* editorial board. The other authors declare that they have no competing interests.

Methods

Cell lines and gene knockdown

HEK293 Flp-In T-REx cells (Thermo Fisher Scientific) were maintained at 5% CO_2 and 37°C in DMEM with high glucose and GlutaMAX supplement (Thermo Fisher Scientific) containing 10% fetal bovine serum (FBS). The cell cultures were routinely tested for contamination with *Mycoplasma* spp. via an e-Myco VALiD Mycoplasma PCR Detection Kit (iNtRON Biotechnology) and were confirmed to be free of infection.

Stable cell lines expressing SBP-eRF1 WT or SBP-eRF1 AAQ mutant were generated (see the "*DNA construction*" section below) via cotransfection of the expression plasmids with pOG44 (Thermo Fisher Scientific) by X-tremeGENE 9 (Sigma–Aldrich) and selected via the addition of hygromycin B (InvivoGen) according to the manufacturer's recommendation.

Gene knockdown was conducted in HEK293 Flp-In T-REx cells via the transfection of siRNAs (ON-TARGETplus/siGENOME SMARTpool, Dharmacon) by TransIT-X2 Dynamic Delivery System (Mirus) according to the manufacturer's recommendation. This study used the following siRNAs: control, D-001810-10-50; ABCE1, L-008702-00-0020; ASCC3, L-012757-01-0010; 4EHP, L-019870-01-0010; and eRF1, M-019840-01-0005. For Thor-Monosome-Seq, Thor-Disome-Seq, and Western blotting, siRNA transfection was conducted twice before the cells were harvested. During the first transfection, a total concentration of 75 nM siRNA was transfected; 50 nM ABCE1 siRNA, 25 nM ASCC3 siRNA, and 25 nM 4EHP siRNA were adjusted with control siRNA to render 75 nM siRNA in total. After 72 h of incubation and cell reseeding, the second siRNA was used at a dose of 30 nM. The cells were incubated for another 24 h and harvested.

For reporter assays, cells were transfected with a total concentration of 75 nM siRNA (25 nM ASCC3 siRNA, 25 nM 4EHP siRNA, or 25 nM eRF1 siRNA) once.

DNA construction

pCDNA5/FRT/TO-SBP-eRF1 WT and AAQ

The DNA fragment encoding eRF1 was PCR-amplified from cDNA generated with total RNA from HEK293 Flp-In T-REx cells as a template and inserted into pCDNA5/FRT/TO-SBP-eIF4A1 [71], replacing eIFA1 with eRF1. AAQ substitution was introduced via site-directed mutagenesis.

psiCHECK2 Nluc-11× CUG, Nluc-11× UUA, and Fluc

Nluc-11× CUG was based on Nluc encoded in pNL1.1 (Promega); Leu24-CUU and Leu32-UUG were converted to CUGs. The synthesized DNA (Eurofins) was inserted into psiCHECK2-GPX1 [71], replacing the *Renilla* luciferase (RLuc)-HSV TK promoter-Fluc region with Nluc-11× CUG and placing the V5 tag at the N-terminus of Nluc-11× CUG.

In Nluc-11× UUA, the CUG codons in Nluc-11× CUG were replaced with UUA codons. The synthesized DNA (Eurofins) was subsequently cloned as described above.

Similarly, DNA fragments encoding Fluc were PCR-amplified from psiCHECK2-GPX1 as a template and subsequently cloned as described above.

eRF1-selective Monosome-Seq and Disome-Seq

Protein expression from stable integrants of SBP-eRF1 WT or AAQ in HEK293 Flp-In T-REx cells was induced with 0.2 μg/ml tetracycline for 2 d before cell harvest. Then, the cells were washed with ice-cold PBS once and lysed with 400 μl of lysis buffer (20 mM

Tris-HCl pH 7.5, 50 mM NaCl, 5 mM $MgCl_2$, 1 mM DTT, 1% Triton X-100, and 100 μg/ml cycloheximide). The cell lysates were treated with 0.0375 U/μl TURBO DNase (Thermo Fisher Scientific) on ice for 10 min and then clarified by centrifugation at 20,000 × *g* at 4°C for 10 min. The supernatants were aliquoted, flash-frozen in liquid nitrogen, and stored at −80°C. RNA concentrations of the cell lysates were determined by a Qubit RNA BR Assay kit (Thermo Fisher Scientific).

The cell lysate containing 6 μg of total RNA was incubated with 70 μl of Dynabeads M-280 Streptavidin (Thermo Fisher Scientific), which was equilibrated with lysis buffer at 4°C for 40 min. The mixture was treated with 3000 U MNase (TaKaRa) with 5 mM $CaCl_2$ at 25°C for 45 min. A fraction of the reaction mixture was used as the input sample.

The reaction mixture was placed on a magnetic stand, and the beads were washed six times with wash buffer (20 mM Tris-HCl pH 7.5, 150 mM NaCl, 5 mM $MgCl_2$, 1 mM DTT, 1% Triton X-100, and 100 μg/ml cycloheximide). Ribosomes bound to SBP-eRF1 were eluted with a wash buffer containing 5 mM biotin. For the input sample after RNase digestion, ribosome complexes were isolated with MicroSpin S-400 HR columns (Cytiva) [46]. RNA was isolated with TRIzol LS (Thermo Fisher Scientific) and a Direct-zol RNA Microprep Kit (Zymo Research).

After PAGE using 15% denatured polyacrylamide SuperSep RNA gels (Fujifilm Wako Pure Chemical Corporation), RNA fragments within the range of 17–34 nt (for Monosome-Seq) and 50–80 nt (for Disome-Seq) were gel-exercised [46]. After dephosphorylation, linker ligation, rRNA depletion via a stand-alone Ribo-Zero Gold rRNA Removal Kit (Human/Mouse/Rat) (Illumina), reverse transcription, circularization,

and PCR amplification [46], the DNA libraries were sequenced via a NovaSeq 6000 (Illumina) with the paired-end/150 nt-long read option.

Thor-Monosome-Seq and Thor-Disome-Seq

siRNA-mediated gene knockdown was performed as described in the "*Cell lines and gene knockdown*" section above. The cells were washed with ice-cold PBS once and then lysed with 400 µl of modified lysis buffer (20 mM Tris-HCl pH 7.5, 150 mM NaCl, 5 mM $MgCl_2$, 1 mM DTT, 1% Triton X-100, 100 µg/ml cycloheximide, 100 µg/ml tigecycline, and 100 µg/ml chloramphenicol). The cell lysates were treated with 0.025 U/µl TURBO DNase (Thermo Fisher Scientific) on ice for 10 min and then clarified by centrifugation at 20,000 × *g* at 4°C for 10 min. The supernatants were aliquoted, flash-frozen in liquid nitrogen, and stored at −80°C. RNA concentration of the cell lysates was determined by a Qubit RNA BR Assay kit (Thermo Fisher Scientific).

The cell lysate containing 3 µg of total RNA was adjusted to 300 µl with modified lysis buffer and treated with 0.067 U/µl RNase I (LGC Biosearch Technologies) at 25°C for 45 min. The reaction was stopped by transferring the mixture to ice, followed by the addition of 200 U SUPERase•In RNase Inhibitor (Thermo Fisher Scientific). The mixture was layered over 900 µl of 1 M sucrose cushion [46] and ultracentrifuged at 100,000 rpm (543,000 × *g*) at 4°C for 1 h using a TLA-110 rotor and an Optima MAX-TL Ultracentrifuge (both Beckman Coulter).

Then, Ribo-FilterOut was conducted [10]. After the supernatant was carefully removed, the ribosome pellet was recovered via the addition of 150 µl pellet lysis buffer (20 mM Tris-HCl pH 7.5, 300 mM NaCl, 5 mM EDTA, 1 mM DTT, 1% Triton X-100, and 0.02 U/µl SUPERase•In RNase Inhibitor) and incubated on ice for 10 min. Ribosome

footprints were further purified by centrifugation at 14,000 × *g* at 4°C for 10 min in a 0.5 ml Amicon Ultra 100 kDa cutoff centrifugal filter unit (Merck Millipore). From the flow-through, RNA was isolated with TRIzol LS (Thermo Fisher Scientific) and a Direct-zol RNA Microprep Kit (Zymo Research). After PAGE using 15% denatured polyacrylamide SuperSep RNA gels (Fujifilm Wako Pure Chemical Corporation), RNA fragments within the range of 17–34 nt (for Monosome-Seq) and 50–80 nt (for Disome-Seq) were gel-exercised [46].

We employed the Thor approach [56] for both Monosome-Seq and Disome-Seq. After dephosphorylation, linker ligation, and rRNA depletion by Ribo-Zero accompanied by a TruSeq Stranded Total RNA Kit (Illumina) [46,56], RNA fragments were amplified via RNA-templated transcription using a T7-Scribe Standard RNA IVT Kit (CELLSCRIPT) for 2.5 h at 37°C [56]. After the second linker was ligated to the 3′ end of the RNA by T4 RNA Ligase 2, truncated K277Q [New England Biolabs (NEB)], cDNA was synthesized using ProtoScript II Reverse Transcriptase (NEB). DNA libraries were generated via PCR with Phusion High-Fidelity DNA Polymerase (NEB), adding barcodes for the Illumina sequencing platform, and sequenced via a NovaSeq 6000 (Illumina) with the paired-end/150 nt-long read option.

RNA-Seq

Total RNA was isolated from the cell lysates used for Thor-Monosome-Seq and Thor-Disome-Seq with TRIzol LS (Thermo Fisher Scientific) and a Direct-zol RNA Microprep kit (Zymo Research). Libraries were constructed using a TruSeq Stranded Total RNA Library Prep Kit (Illumina) and sequenced with a NovaSeq 6000 (Illumina) with the paired-end/150 nt-long read option.

Deep sequencing data analysis

Paired-end reads were corrected by fastp (ver. 0.21.0) [72]. The R1 data were subsequently used for downstream analysis. The adaptor sequences were trimmed with fastp (ver. 0.21.0) [72]. Reads that were aligned to noncoding RNA by STAR (ver. 2.7.0a) [73] were excluded. The remaining reads were aligned to the hg38 genome (GENCODE v32 annotation) via STAR (ver. 2.7.0a) [73]. Duplicated reads that occurred during *in vitro* transcription by T7 polymerase were suppressed by UMI via UMI-tools (ver. 1.1.4) [74]. Transcripts that were defined in the Ensembl canonical transcript list and had a complete CDS and a canonical stop codon were used for the analysis.

Monosome and disome occupancies at each codon were determined by normalizing the raw reads at each given codon to the average number of footprints per codon on the transcript. Transcripts that had less than 0.2 footprints per codon were excluded from the analysis. Codons that had fewer than two mapped reads were also excluded. Codons whose disome occupancy was the value of the mean + s.d. or larger were defined as disome pause sites.

The differential expression of RNA and translation efficiency were analyzed via DESeq2 (ver. 1.28.1) [75].

Western blotting

The concentration of total protein in the cell lysates was adjusted. After 2× SDS sample buffer (125 mM Tris-HCl pH 6.8, 20% glycerol, 4% SDS, 10% 2-mercaptoethanol, and 0.004% BPB) was added, the samples were heated at 95°C for 5 min. Electrophoresis of the protein samples was performed via 5–20% Tris–glycine SDS–PAGE gels (Gellex).

Proteins were subsequently transferred to 0.2-μm nitrocellulose membranes via a Trans-Blot Turbo Transfer System (Bio-Rad). The membranes were blocked with TBS blocking buffer (LI-COR Biosciences) for 1 h at room temperature.

The primary antibodies used were anti-ABCE1 (Abcam, ab185548, 1:1000), anti-ASCC3 (PROTEINTECH, 17627-1-AP, 1:500), anti-4EHP (Cell Signaling Technology, 6916S, 1:250), and β-actin (LI-COR Biosciences, 926-42210, 1:1000). The following secondary antibodies were used: IRDye 800CW anti-rabbit IgG (LI-COR Biosciences, #926-32211, 1:10000) and IRDye 800CW anti-mouse IgG (LI-COR Biosciences, #926-32210, 1:10000). The membranes were imaged via an ODYSSEY CLx system (LI-COR Biosciences).

Preparation of reporter mRNAs

The DNA fragments encoding the Nuc and Fluc reporters were PCR-amplified with the primers 5′-TGACTAATACGACTCACTATAGG-3′ and 5′-TGTATCTTATCATGTCTGCTCGAAG-3′ using psiCHECK2-Nluc-11× CUG, 11× UUA, and Fluc as templates. Using these DNA fragments as templates, *in vitro* transcription was conducted with a T7-Scribe Standard RNA IVT Kit (CELLSCRIPT) for 2 h at 37°C. Capping and polyadenylation were conducted using a ScriptCap m^7G Capping Kit (CELLSCRIPT), a ScriptCap 2′-*O*-Methyltransferase Kit (CELLSCRIPT), and an A-Plus Poly (A) Polymerase Tailing Kit (CELLSCRIPT).

Reporter assay with an in vitro translation system

In vitro translation of the reporter mRNAs (0.125 μM Fluc mRNA and 0.25 μM Nluc mRNA) was performed with Rabbit Reticulocyte Lysate [Nuclease-Treated] (Promega)

at 30°C for 30 min. The indicated amount of eRF1-eRF3 recombinant proteins, which were prepared as previously described [76], were added to the reactions. The reaction was stopped by adding 1× Passive Lysis Buffer (Promega). A dual-luciferase reporter assay was performed via a Nano-Glo Dual-Luciferase Reporter Assay System (Promega) and a GloMax Navigator Microplate Luminometer (Promega).

Reporter assay in cells

HEK293 Flp-In T-REx cells were transfected as described in the "*Cell lines and gene knockdown*" section. After siRNA transfection and 30 h incubation, the cells were reseeded to a Nunc MicroWell 96-well Microplate (Thermo Fisher Scientific) and incubated for 18 h. For each well, 0.02 μg Fluc mRNA and 0.02 μg Nluc mRNA were transfected with a TransIT-mRNA Transfection Kit (Mirus) and incubated for 4 h. A dual-luciferase reporter assay was performed via a Nano-Glo Dual-Luciferase Reporter Assay System (Promega) and a GloMax Navigator Microplate Luminometer (Promega).

Data availability

The Monosome-Seq, Disome-Seq, and RNA-Seq data (GSE275336) [https://www.ncbi.nlm.nih.gov/geo/query/acc.cgi?acc=GSE275336] obtained in this study were deposited in the National Center for Biotechnology Information (NCBI) database. Gene annotations (GENCODE Human Release 32 reference) were obtained via the UCSC Genome Browser (https://genome.ucsc.edu/index.html).

Code availability

The custom scripts used in this study are available at Zenodo (DOI: 10.5281/zenodo.13352233) [https://zenodo.org/doi/10.5281/zenodo.13352233] [77].

Figure and table legends

Figure 1. eRF1 transiently associates with UUA sense codons and leads to ribosome collision.

(A) Schematic of eRF1-selective Monosome-Seq and Disome-Seq.

(B) Metagene plot of the relative monosome footprint distribution (monosome occupancy) around stop codons.

(C) Monosome occupancy differences between the eRF1 WT-bound fraction and the input. The data for the top 15 codons are shown. See Figure S1C for the full data.

(D) Disome occupancy differences between the eRF1 WT-bound fraction and the input. The data for the top 15 codons are shown. See Figure S1E for the full data.

(E) Metagene plot of the relative disome footprint distribution (disome occupancy; a site of the leading ribosome) around UUA codons.

(F) Metagene plot of disome occupancy around stop codons for the indicated conditions.

(G) Metagene plot of disome occupancy around UUA codons for the indicated conditions.

(H) Disome occupancy difference between the eRF1 AAQ-bound fraction and the input. The data for the top 15 codons are shown. See Figure S3C for the full data.

See also Figures S1-3.

Figure 2. eRF1 delays ribosome elongation at UUA codons.

(A) *In vitro* translation assay using RRL for the Nluc-11× CUG and 11× UUA reporters. A titrated amount of the recombinant eRF1-eRF3 complex was added to the reactions. The data are presented as the means (bars) and s.d.s (errors) for replicates (points, n = 3).

(B) Comparison of monosome occupancy (left) and disome occupancy (right) on A-site codons (for disomes, A-site codons for the leading ribosomes) for the indicated conditions.

(C) Distribution of monosome footprint length at the indicated codon positions.

Figure 3. Disomes on UUA codons are rescued by RQC.

(A) Schematic of the functions of RQC factors whose expression was knocked down in this study.

(B and D) Comparison of disome occupancy on A-site codons (for disomes, A-site codons for the leading ribosomes) for the indicated conditions.

(C) Metagene plot of disome occupancy around UUA codons for the indicated conditions.

(E) A breakdown of disome pause sites, illustrating the proportions of the indicated categories. The p values were calculated via two-sided Pearson's chi-square test.

(F) Distribution of disome footprints along the indicated genes. The A-site position of the leading ribosome is depicted.

(G) In-cell reporter assay using the Nluc-11× CUG and 11× UUA reporters. The indicated genes were knocked down. The data are presented as the means (bars) and s.d.s (errors) for replicates (points, n = 3).

See also Figures S2 and S4.

Figure 4. Depletion of RQC factors activates alternative pathways that sense disomes.

(A) Western blotting of the indicated proteins. Vinculin was used as a loading control. Representative data from three replicate experiments are shown.

(B) MA (M, log ratio; A, mean average) plot for RNA abundance change, measured by RNA-Seq, with ASCC3-4EHP double knockdown. Transcripts with significant changes (FDR < 0.05) are shown.

(C) Heatmap of RNA abundance change for the indicated genes under the indicated conditions. The color scales for the fold changes are shown.

(D) Schematic of the model of eRF1-mediated UUA codon association, ribosome collision, and subsequent rescue by RQC.

Figure S1. Characterization of eRF1-selective Monosome-Seq and Disome-Seq data, related to Figure 1.

(A) Western blotting results for the indicated proteins. β-Actin was used as a loading control.

(B and D) Distribution of monosome (B) and disome (D) footprint lengths under the indicated conditions.

(C and E) Monosome (C) and disome (E) occupancy differences between the eRF1 WT-bound fraction and the input.

(F) Disome occupancy differences between the eRF1 WT-bound fraction and the input for the indicated codon context.

Figure S2. Characterization of Thor-Monosome-Seq and Thor-Disome-Seq data upon gene knockdown, related to Figures 1 and 3.

(A) Fractions of usable reads for the indicated conditions for Disome-Seq library preparation. The DASH-treated data have previously been reported [28].

(B and E) Western blotting results for the indicated proteins. β-Actin (B) and vinculin (E) were used as loading controls.

(C-D) Distribution of monosome (C) and disome (D) footprint lengths under the indicated conditions.

Figure S3. Effects of the eRF1 AAQ mutation on eRF1-selective Monosome-Seq and Disome-Seq data, related to Figure 1.

(A) Schematic of the outcome of eRF1 (WT or AAQ mutant) association with the sense UUA codon and stop codon.

(B and C) Monosome (B) and disome (C) occupancy differences between the eRF1 AAQ-bound fraction and the input.

(D) The folded four-base structure of mRNA in the A site of the 80S•eRF1•eRF3 complex (PDB ID: 5LZT)[37]. The hydrogen bonds are indicated by cyan dotted lines, and the interaction between Mg^{2+} and N7 of G+2 is indicated by a gray dotted line.

Figure S4. RQC does not rescue disomes on poly-Lys motifs in human cells, related to Figure 3.

(A) Distribution of disome footprints along the indicated genes. The A-site position of the leading ribosome is depicted. The Lys-rich region is highlighted.

(B) Comparison of disome occupancy on P- and A-site codon combinations (for disomes, A-site codons for the leading ribosomes) for the indicated conditions. The data were aggregated into amino acid pairs.

References

1. D'Orazio, K.N., and Green, R. (2021). Ribosome states signal RNA quality control. Mol. Cell *81*, 1372–1383.

2. Yip, M.C.J., and Shao, S. (2021). Detecting and rescuing stalled ribosomes. Trends Biochem. Sci. *46*, 731–743.

3. Filbeck, S., Cerullo, F., Pfeffer, S., and Joazeiro, C.A.P. (2022). Ribosome-associated quality-control mechanisms from bacteria to humans. Mol. Cell *82*, 1451–1466.

4. Kim, K.Q., and Zaher, H.S. (2022). Canary in a coal mine: collided ribosomes as sensors of cellular conditions. Trends Biochem. Sci. *47*, 82–97.

5. Morisaki, T., Lyon, K., DeLuca, K.F., DeLuca, J.G., English, B.P., Zhang, Z., Lavis, L.D., Grimm, J.B., Viswanathan, S., Looger, L.L., et al. (2016). Real-time quantification of single RNA translation dynamics in living cells. Science *352*, 1425–1429.

6. Yan, X., Hoek, T.A., Vale, R.D., and Tanenbaum, M.E. (2016). Dynamics of translation of single mRNA molecules *in vivo*. Cell *165*, 976–989.

7. Wang, C., Han, B., Zhou, R., and Zhuang, X. (2016). Real-time imaging of translation on single mRNA transcripts in live cells. Cell *165*, 990–1001.

8. Wu, B., Eliscovich, C., Yoon, Y.J., and Singer, R.H. (2016). Translation dynamics of single mRNAs in live cells and neurons. Science *352*, 1430–1435.

9. Voigt, F., Zhang, H., Cui, X.A., Triebold, D., Liu, A.X., Eglinger, J., Lee, E.S., Chao, J.A., and Palazzo, A.F. (2017). Single-molecule quantification of translation-dependent association of mRNAs with the endoplasmic reticulum. Cell Rep. *21*, 3740–3753.

10. Tomuro, K., Mito, M., Toh, H., Kawamoto, N., Miyake, T., Chow, S.Y.A., Doi, M., Ikeuchi, Y., Shichino, Y., and Iwasaki, S. (2024). Calibrated ribosome profiling assesses the dynamics of ribosomal flux on transcripts. Nat. Commun. *15*, 7061.

11. Brandman, O., Stewart-Ornstein, J., Wong, D., Larson, A., Williams, C.C., Li, G.W., Zhou, S., King, D., Shen, P.S., Weibezahn, J., et al. (2012). A ribosome-bound quality control complex triggers degradation of nascent peptides and signals translation stress. Cell *151*, 1042–1054.

12. Juszkiewicz, S., and Hegde, R. (2017). Initiation of quality control during poly(A) translation requires site-specific ribosome ubiquitination. Mol. Cell *65*, 743–750.e4.

13. Matsuo, Y., Ikeuchi, K., Saeki, Y., Iwasaki, S., Schmidt, C., Udagawa, T., Sato, F., Tsuchiya, H., Becker, T., Tanaka, K., et al. (2017). Ubiquitination of stalled ribosome triggers ribosome-associated quality control. Nat. Commun. *8*, 159.

14. Sundaramoorthy, E., Leonard, M., Mak, R., Liao, J., Fulzele, A., and Bennett, E.J. (2017). ZNF598 and RACK1 regulate mammalian ribosome-associated quality control function by mediating regulatory 40S ribosomal ubiquitylation. Mol. Cell *65*, 751–760.e4.

15. Juszkiewicz, S., Chandrasekaran, V., Lin, Z., Kraatz, S., Ramakrishnan, V., and Hegde, R.S. (2018). ZNF598 is a quality control sensor of collided ribosomes. Mol. Cell *72*, 469–481.e7.

16. Ikeuchi, K., Tesina, P., Matsuo, Y., Sugiyama, T., Cheng, J., Saeki, Y., Tanaka, K., Becker, T., Beckmann, R., and Inada, T. (2019). Collided ribosomes form a unique structural interface to induce Hel2-driven quality control pathways. EMBO J. *38*, e100276.

17. Matsuo, Y., Tesina, P., Nakajima, S., Mizuno, M., Endo, A., Buschauer, R., Cheng, J., Shounai, O., Ikeuchi, K., Saeki, Y., et al. (2020). RQT complex dissociates ribosomes collided on endogenous RQC substrate SDD1. Nat. Struct. Mol. Biol. *27*, 323–332.

18. Narita, M., Denk, T., Matsuo, Y., Sugiyama, T., Kikuguchi, C., Ito, S., Sato, N., Suzuki, T., Hashimoto, S., Machová, I., et al. (2022). A distinct mammalian disome collision interface harbors K63-linked polyubiquitination of uS10 to trigger hRQT-mediated subunit dissociation. Nat. Commun. *13*, 6411.

19. Juszkiewicz, S., Speldewinde, S.H., Wan, L., Svejstrup, J.Q., and Hegde, R.S. (2020). The ASC-1 complex disassembles collided ribosomes. Mol. Cell *79*, 603–614.e8.

20. Best, K., Ikeuchi, K., Kater, L., Best, D., Musial, J., Matsuo, Y., Berninghausen, O., Becker, T., Inada, T., and Beckmann, R. (2023). Structural basis for clearing of ribosome collisions by the RQT complex. Nat. Commun. *14*, 921.

21. Miścicka, A., Bulakhov, A.G., Kuroha, K., Zinoviev, A., Hellen, C.U.T., and Pestova, T.V. (2024). Ribosomal collision is not a prerequisite for ZNF598-mediated ribosome ubiquitination and disassembly of ribosomal complexes by ASCC. Nucleic Acids Res. *52*, 4627–4643.

22. Tollenaere, M.A.X., Tiedje, C., Rasmussen, S., Nielsen, J.C., Vind, A.C., Blasius, M., Batth, T.S., Mailand, N., Olsen, J.V., Gaestel, M., et al. (2019). GIGYF1/2-driven cooperation between ZNF598 and TTP in posttranscriptional regulation of inflammatory signaling. Cell Rep. *26*, 3511–3521.e4.

23. Juszkiewicz, S., Slodkowicz, G., Lin, Z., Freire-Pritchett, P., Peak-Chew, S.-Y., and Hegde, R.S. (2020). Ribosome collisions trigger cis-acting feedback inhibition of translation initiation. Elife *9*, e60038.

24. Hickey, K.L., Dickson, K., Cogan, J.Z., Replogle, J.M., Schoof, M., D'Orazio, K.N., Sinha, N.K., Hussmann, J.A., Jost, M., Frost, A., et al. (2020). GIGYF2 and 4EHP inhibit translation initiation of defective messenger RNAs to assist ribosome-associated quality control. Mol. Cell *79*, 950–962.e6.

25. Sinha, N.K., Ordureau, A., Best, K., Saba, J.A., Zinshteyn, B., Sundaramoorthy, E., Fulzele, A., Garshott, D.M., Denk, T., Thoms, M., et al. (2020). EDF1 coordinates cellular responses to ribosome collisions. Elife *9*, e58828.

26. Weber, R., Chung, M.-Y., Keskeny, C., Zinnall, U., Landthaler, M., Valkov, E., Izaurralde, E., and Igreja, C. (2020). 4EHP and GIGYF1/2 mediate translation-coupled messenger RNA decay. Cell Rep. *33*, 108262.

27. Ito-Harashima, S., Kuroha, K., Tatematsu, T., and Inada, T. (2007). Translation of the poly(A) tail plays crucial roles in nonstop mRNA surveillance via translation repression and protein destabilization by proteasome in yeast. Genes Dev. *21*, 519–524.

28. Han, P., Shichino, Y., Schneider-Poetsch, T., Mito, M., Hashimoto, S., Udagawa, T., Kohno, K., Yoshida, M., Mishima, Y., Inada, T., et al. (2020). Genome-wide survey of ribosome collision. Cell Rep. *31*, 107610.

29. Wu, Z., Tantray, I., Lim, J., Chen, S., Li, Y., Davis, Z., Sitron, C., Dong, J., Gispert, S., Auburger, G., et al. (2019). MISTERMINATE mechanistically links mitochondrial dysfunction with proteostasis failure. Mol. Cell *75*, 835–848.e8.

30. Meydan, S., and Guydosh, N.R. (2020). Disome and trisome profiling reveal genome-wide targets of ribosome quality control. Mol. Cell *79*, 588–602.e6.

31. Stein, K.C., Morales-Polanco, F., van der Lienden, J., Rainbolt, T.K., and Frydman, J. (2022). Ageing exacerbates ribosome pausing to disrupt cotranslational proteostasis. Nature *601*, 637–642.

32. Yan, L.L., Simms, C.L., McLoughlin, F., Vierstra, R.D., and Zaher, H.S. (2019). Oxidation and alkylation stresses activate ribosome-quality control. Nat. Commun. *10*, 5611.

33. Zhao, T., Chen, Y.M., Li, Y., Wang, J., Chen, S., Gao, N., and Qian, W. (2021). Disome-seq reveals widespread ribosome collisions that promote cotranslational protein folding. Genome Biol. *22*, 16.

34. Hellen, C.U.T. (2018). Translation termination and ribosome recycling in eukaryotes. Cold Spring Harb. Perspect. Biol. *10*, a032656.

35. Brown, A., Shao, S., Murray, J., Hegde, R.S., and Ramakrishnan, V. (2015). Structural basis for stop codon recognition in eukaryotes. Nature *524*, 493–496.

36. Matheisl, S., Berninghausen, O., Becker, T., and Beckmann, R. (2015). Structure of a human translation termination complex. Nucleic Acids Res. *43*, 8615–8626.

37. Shao, S., Murray, J., Brown, A., Taunton, J., Ramakrishnan, V., and Hegde, R.S. (2016). Decoding mammalian ribosome-mRNA states by translational GTPase complexes. Cell *167*, 1229–1240.e15.

38. Lawson, M.R., Lessen, L.N., Wang, J., Prabhakar, A., Corsepius, N.C., Green, R., and Puglisi, J.D. (2021). Mechanisms that ensure speed and fidelity in eukaryotic translation termination. Science *373*, 876–882.

39. Wada, M., and Ito, K. (2019). Misdecoding of rare CGA codon by translation termination factors, eRF1/eRF3, suggests novel class of ribosome rescue pathway in *S. cerevisiae*. FEBS J. *286*, 788–802.

40. Yang, Q., Yu, C.-H., Zhao, F., Dang, Y., Wu, C., Xie, P., Sachs, M.S., and Liu, Y. (2019). eRF1 mediates codon usage effects on mRNA translation efficiency through premature termination at rare codons. Nucleic Acids Res. *47*, 9243–9258.

41. Oh, E., Becker, A.H., Sandikci, A., Huber, D., Chaba, R., Gloge, F., Nichols, R.J., Typas, A., Gross, C.A., Kramer, G., et al. (2011). Selective ribosome profiling reveals the cotranslational chaperone action of trigger factor *in vivo*. Cell *147*,

1295–1308.

42. Günnigmann, M., Koubek, J., Kramer, G., and Bukau, B. (2023). Selective ribosome profiling as a tool to study interactions of translating ribosomes in mammalian cells. Methods Enzymol. *684*, 1–38.

43. Miettinen, T.P., and Björklund, M. (2015). Modified ribosome profiling reveals high abundance of ribosome protected mRNA fragments derived from 3′ untranslated regions. Nucleic Acids Res. *43*, 1019–1034.

44. McGlincy, N.J., and Ingolia, N.T. (2017). Transcriptome-wide measurement of translation by ribosome profiling. Methods *126*, 112–129.

45. Shirokikh, N.E., Archer, S.K., Beilharz, T.H., Powell, D., and Preiss, T. (2017). Translation complex profile sequencing to study the in vivo dynamics of mRNA–ribosome interactions during translation initiation, elongation and termination. Nat. Protoc. *12*, 697–731.

46. Mito, M., Mishima, Y., and Iwasaki, S. (2020). Protocol for disome profiling to survey ribosome collision in humans and zebrafish. STAR Protoc *1*, 100168.

47. Wagner, S., Bohlen, J., Herrmannova, A., Jelínek, J., Preiss, T., Valášek, L.S., and Teleman, A.A. (2022). Selective footprinting of 40S and 80S ribosome subpopulations (Sel-TCP-seq) to study translation and its control. Nat. Protoc. *17*, 2139–2187.

48. Wu, C.C., Zinshteyn, B., Wehner, K.A., and Green, R. (2019). High-resolution ribosome profiling defines discrete ribosome elongation states and translational

regulation during cellular stress. Mol. Cell *73*, 959–970.e5.

49. Guydosh, N.R., and Green, R. (2014). Dom34 rescues ribosomes in 3′ untranslated regions. Cell *156*, 950–962.

50. Arpat, A.B., Liechti, A., De Matos, M., Dreos, R., Janich, P., and Gatfield, D. (2020). Transcriptome-wide sites of collided ribosomes reveal principles of translational pausing. Genome Res. *30*, 985–999.

51. Young, D.J., Guydosh, N.R., Zhang, F., Hinnebusch, A.G., and Green, R. (2015). Rli1/ABCE1 recycles terminating ribosomes and controls translation reinitiation in 3′ UTRs *in vivo*. Cell *162*, 872–884.

52. Mills, E.W., Wangen, J., Green, R., and Ingolia, N.T. (2016). Dynamic regulation of a ribosome rescue pathway in erythroid cells and platelets. Cell Rep. *17*, 1–10.

53. Sudmant, P.H., Lee, H., Dominguez, D., Heiman, M., and Burge, C.B. (2018). Widespread accumulation of ribosome-associated isolated 3’ UTRs in neuronal cell populations of the aging brain. Cell Rep. *25*, 2447–2456.e4.

54. Annibaldis, G., Domanski, M., Dreos, R., Contu, L., Carl, S., Kläy, N., and Mühlemann, O. (2020). Readthrough of stop codons under limiting ABCE1 concentration involves frameshifting and inhibits nonsense-mediated mRNA decay. Nucleic Acids Res. *48*, 10259–10279.

55. Zhu, X., Zhang, H., and Mendell, J.T. (2020). Ribosome recycling by ABCE1 links lysosomal function and iron homeostasis to 3′ UTR-directed regulation and nonsense-mediated decay. Cell Rep. *32*, 107895.

56. Mito, M., Shichino, Y., and Iwasaki, S. (2023). Thor-Ribo-Seq: ribosome profiling tailored for low input with RNA-dependent RNA amplification. bioRxiv, 2023.01.15.524129. https://doi.org/10.1101/2023.01.15.524129.

57. Frolova, L.Y., Tsivkovskii, R.Y., Sivolobova, G.F., Oparina, N.Y., Serpinsky, O.I., Blinov, V.M., Tatkov, S.I., and Kisselev, L.L. (1999). Mutations in the highly conserved GGQ motif of class 1 polypeptide release factors abolish ability of human eRF1 to trigger peptidyl-tRNA hydrolysis. RNA *5*, 1014–1020.

58. Preis, A., Heuer, A., Barrio-Garcia, C., Hauser, A., Eyler, D.E., Berninghausen, O., Green, R., Becker, T., and Beckmann, R. (2014). Cryoelectron microscopic structures of eukaryotic translation termination complexes containing eRF1-eRF3 or eRF1-ABCE1. Cell Rep. *8*, 59–65.

59. Ingolia, N.T., Lareau, L.F., and Weissman, J.S. (2011). Ribosome profiling of mouse embryonic stem cells reveals the complexity and dynamics of mammalian proteomes. Cell *147*, 789–802.

60. Arthur, L., Pavlovic-Djuranovic, S., Smith-Koutmou, K., Green, R., Szczesny, P., and Djuranovic, S. (2015). Translational control by lysine-encoding A-rich sequences. Sci Adv *1*, e1500154.

61. Vind, A.C., Snieckute, G., Blasius, M., Tiedje, C., Krogh, N., Bekker-Jensen, D.B., Andersen, K.L., Nordgaard, C., Tollenaere, M.A.X., Lund, A.H., et al. (2020). ZAKα recognizes stalled ribosomes through partially redundant sensor domains. Mol. Cell *78*, 700–713.e7.

62. Wu, C.C.-C., Peterson, A., Zinshteyn, B., Regot, S., and Green, R. (2020). Ribosome collisions trigger general stress responses to regulate cell fate. Cell *182*, 404–416.e14.

63. Snieckute, G., Genzor, A.V., Vind, A.C., Ryder, L., Stoneley, M., Chamois, S., Dreos, R., Nordgaard, C., Sass, F., Blasius, M., et al. (2022). Ribosome stalling is a signal for metabolic regulation by the ribotoxic stress response. Cell Metab. *34*, 2036–2046.e8.

64. Stoneley, M., Harvey, R.F., Mulroney, T.E., Mordue, R., Jukes-Jones, R., Cain, K., Lilley, K.S., Sawarkar, R., and Willis, A.E. (2022). Unresolved stalled ribosome complexes restrict cell-cycle progression after genotoxic stress. Mol. Cell *82*, 1557–1572.e7.

65. Zhao, S., Cordes, J., Caban, K.M., Götz, M.J., Mackens-Kiani, T., Veltri, A.J., Sinha, N.K., Weickert, P., Kaya, S., Hewitt, G., et al. (2023). RNF14-dependent atypical ubiquitylation promotes translation-coupled resolution of RNA-protein crosslinks. Mol. Cell *83*, 4290–4303.e9.

66. Sinha, N.K., McKenney, C., Yeow, Z.Y., Li, J.J., Nam, K.H., Yaron-Barir, T.M., Johnson, J.L., Huntsman, E.M., Cantley, L.C., Ordureau, A., et al. (2024). The ribotoxic stress response drives UV-mediated cell death. Cell *187*, 3652–3670.e40.

67. Yan, L.L., and Zaher, H.S. (2021). Ribosome quality control antagonizes the activation of the integrated stress response on colliding ribosomes. Mol. Cell *81*, 614–628.e4.

68. Subramanian, A., Wang, L., Moss, T., Voorhies, M., Sangwan, S., Stevenson, E., Pulido, E.H., Kwok, S., Chalkley, R.J., Li, K.H., et al. (2023). A *Legionella* toxin exhibits tRNA mimicry and glycosyl transferase activity to target the translation machinery and trigger a ribotoxic stress response. Nat. Cell Biol. *25*, 1600–1615.

69. Han, H., Cho, J.-W., Lee, S., Yun, A., Kim, H., Bae, D., Yang, S., Kim, C.Y., Lee, M., Kim, E., et al. (2018). TRRUST v2: an expanded reference database of human and mouse transcriptional regulatory interactions. Nucleic Acids Res. *46*, D380–D386.

70. Holm, M., Natchiar, S.K., Rundlet, E.J., Myasnikov, A.G., Watson, Z.L., Altman, R.B., Wang, H.-Y., Taunton, J., and Blanchard, S.C. (2023). mRNA decoding in human is kinetically and structurally distinct from bacteria. Nature *617*, 200–207.

71. Iwasaki, S., Floor, S.N., and Ingolia, N.T. (2016). Rocaglates convert DEAD-box protein eIF4A into a sequence-selective translational repressor. Nature *534*, 558–561.

72. Chen, S., Zhou, Y., Chen, Y., and Gu, J. (2018). fastp: an ultra-fast all-in-one FASTQ preprocessor. Bioinformatics *34*, i884–i890.

73. Dobin, A., Davis, C.A., Schlesinger, F., Drenkow, J., Zaleski, C., Jha, S., Batut, P., Chaisson, M., and Gingeras, T.R. (2013). STAR: ultrafast universal RNA-seq aligner. Bioinformatics *29*, 15–21.

74. Smith, T., Heger, A., and Sudbery, I. (2017). UMI-tools: modeling sequencing errors in Unique Molecular Identifiers to improve quantification accuracy. Genome

Res. *27*, 491–499.

75. Love, M.I., Huber, W., and Anders, S. (2014). Moderated estimation of fold change and dispersion for RNA-seq data with DESeq2. Genome Biol. *15*, 550.

76. Machida, K., Mikami, S., Masutani, M., Mishima, K., Kobayashi, T., and Imataka, H. (2014). A translation system reconstituted with human factors proves that processing of encephalomyocarditis virus proteins 2A and 2B occurs in the elongation phase of translation without eukaryotic release factors. J. Biol. Chem. *289*, 31960–31971.

77. Han, P. (2028). Sense codon-misassociated eRF1 elicits widespread ribosome stalling subjected to quality control. https://doi.org/10.5281/ZENODO.13352233.

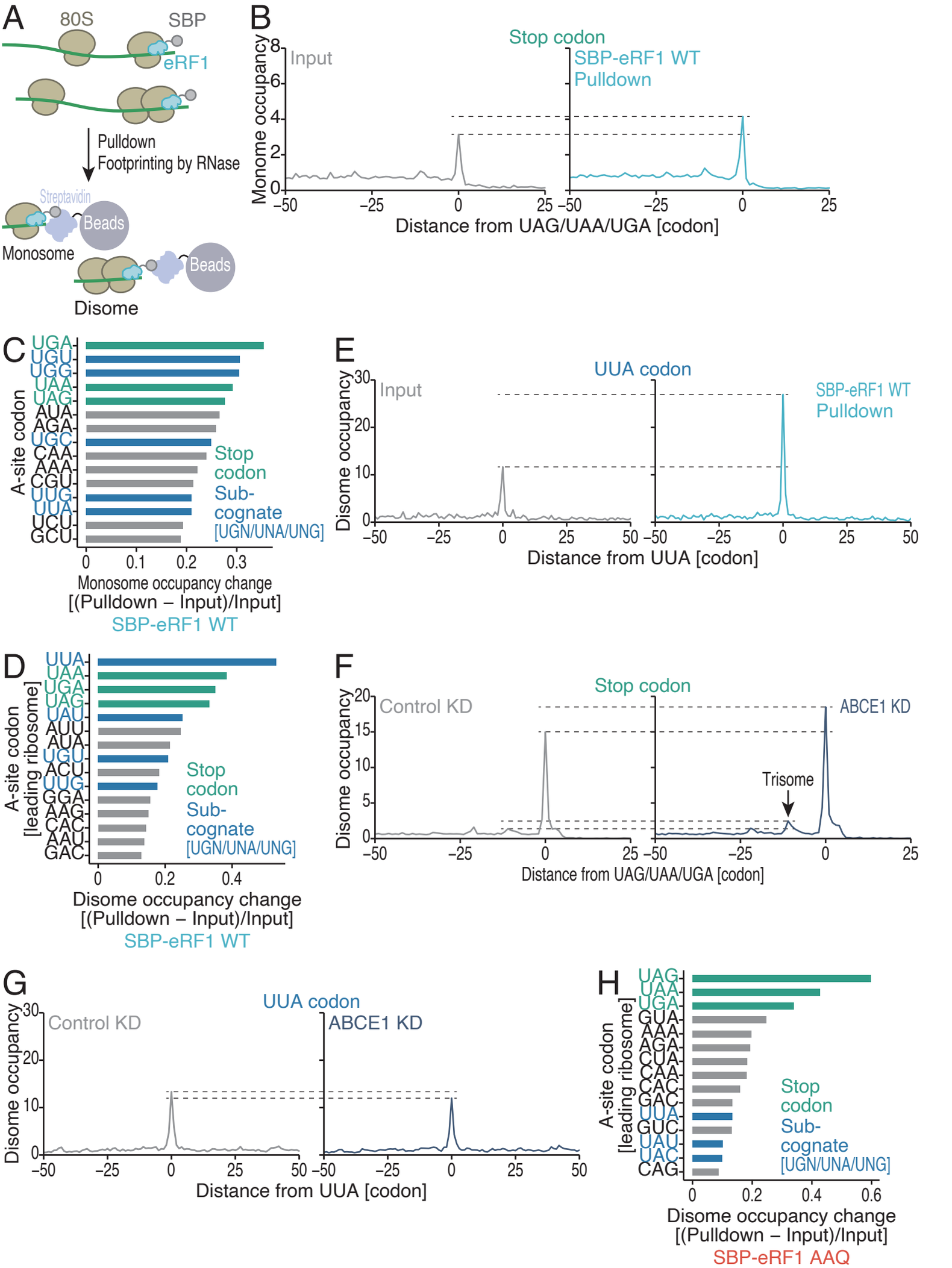

Figure 1 Han *et al.* (2024)

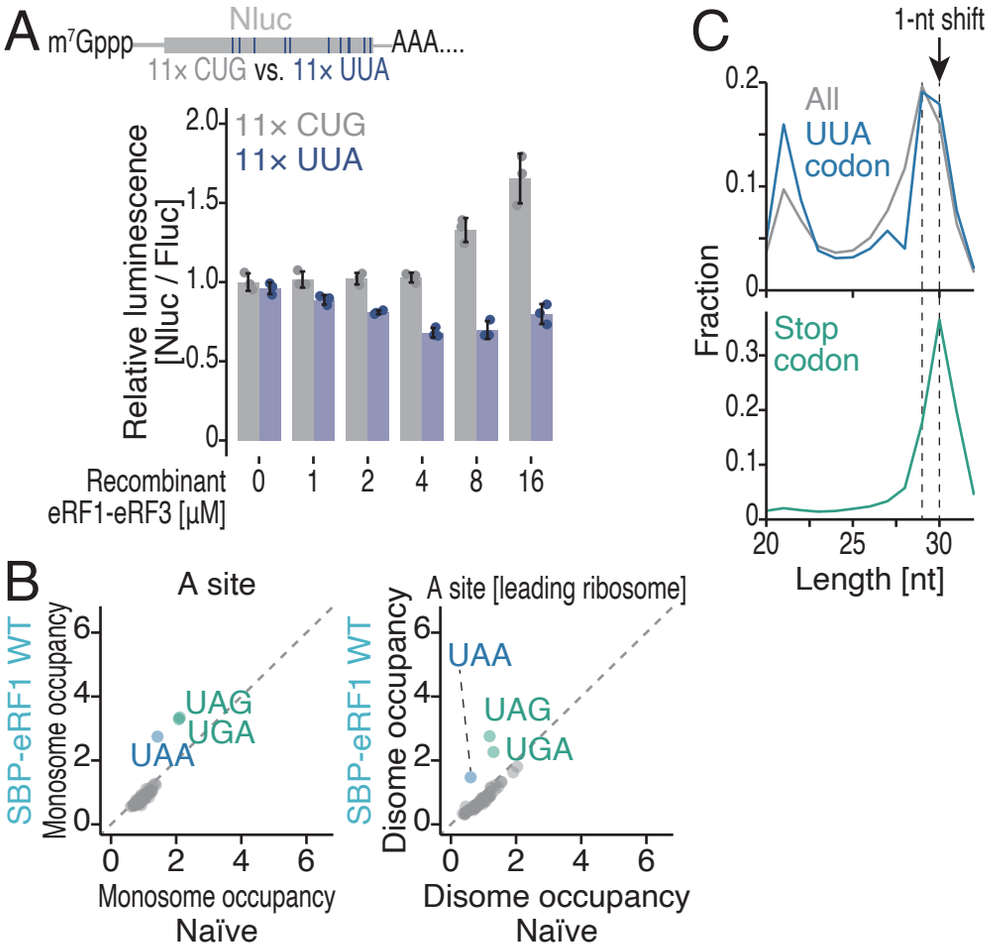

Figure 2 Han *et al.* (2024)

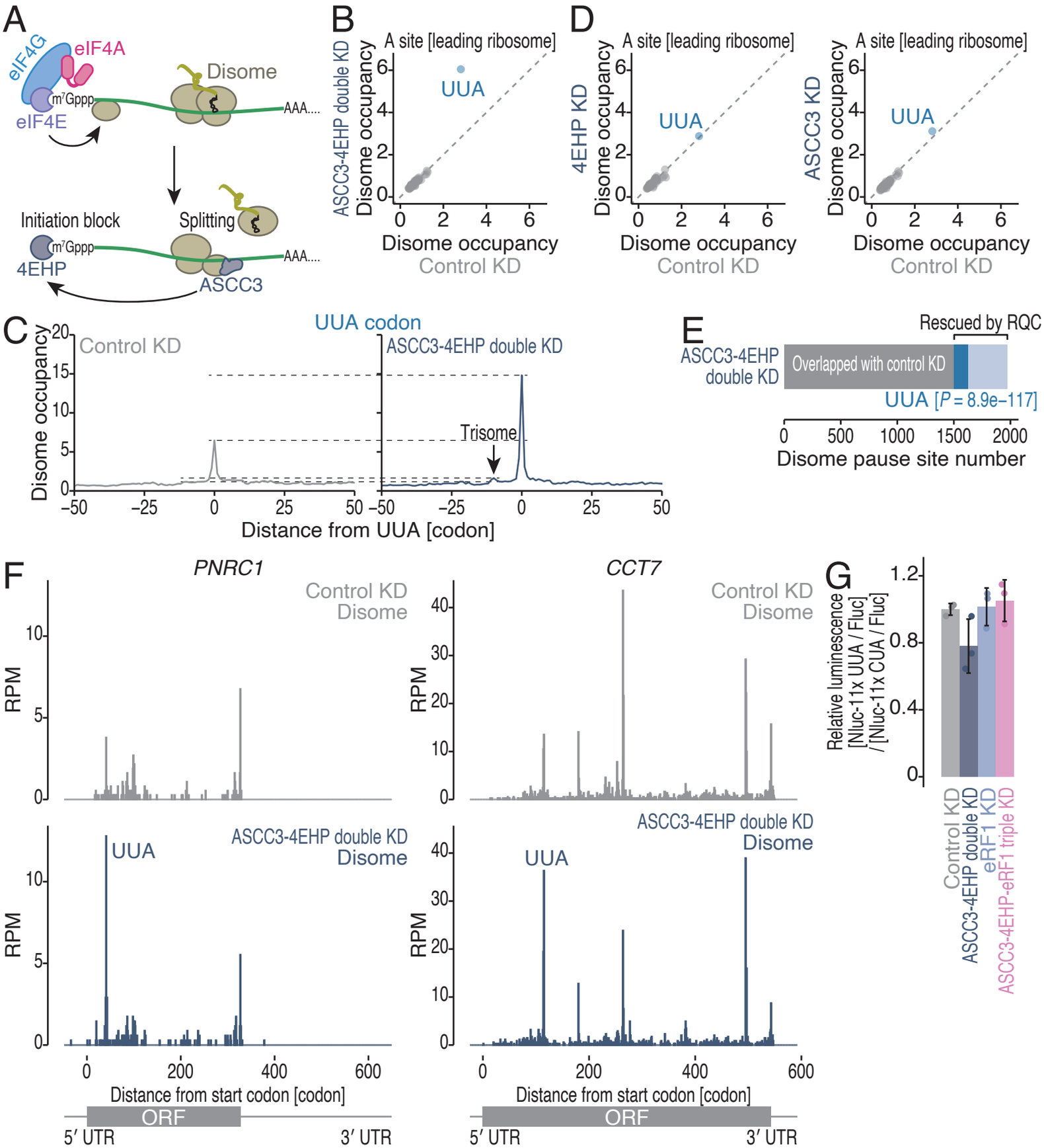

Figure 3 Han *et al.* (2024)

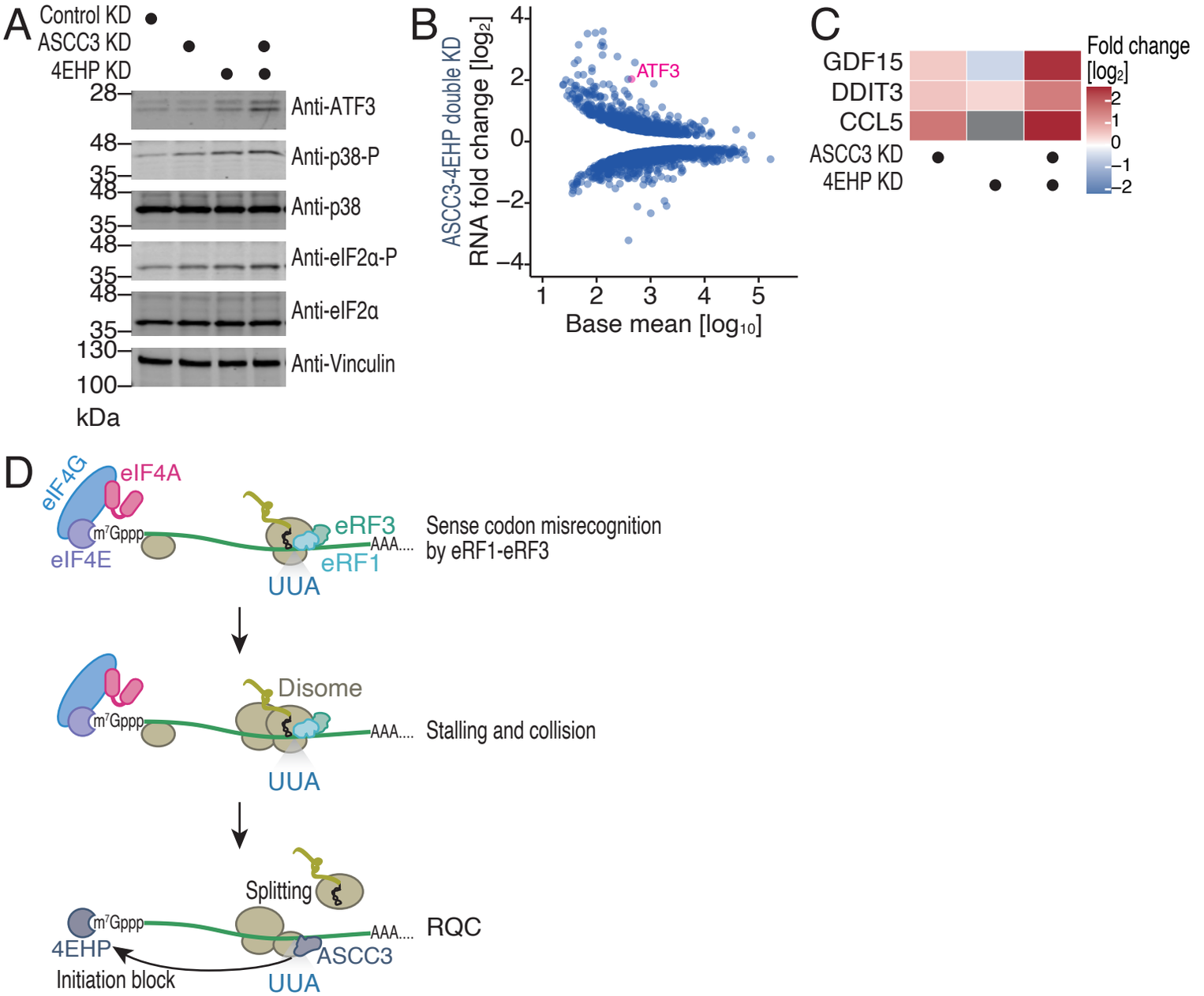

Figure 4 Han *et al.* (2024)

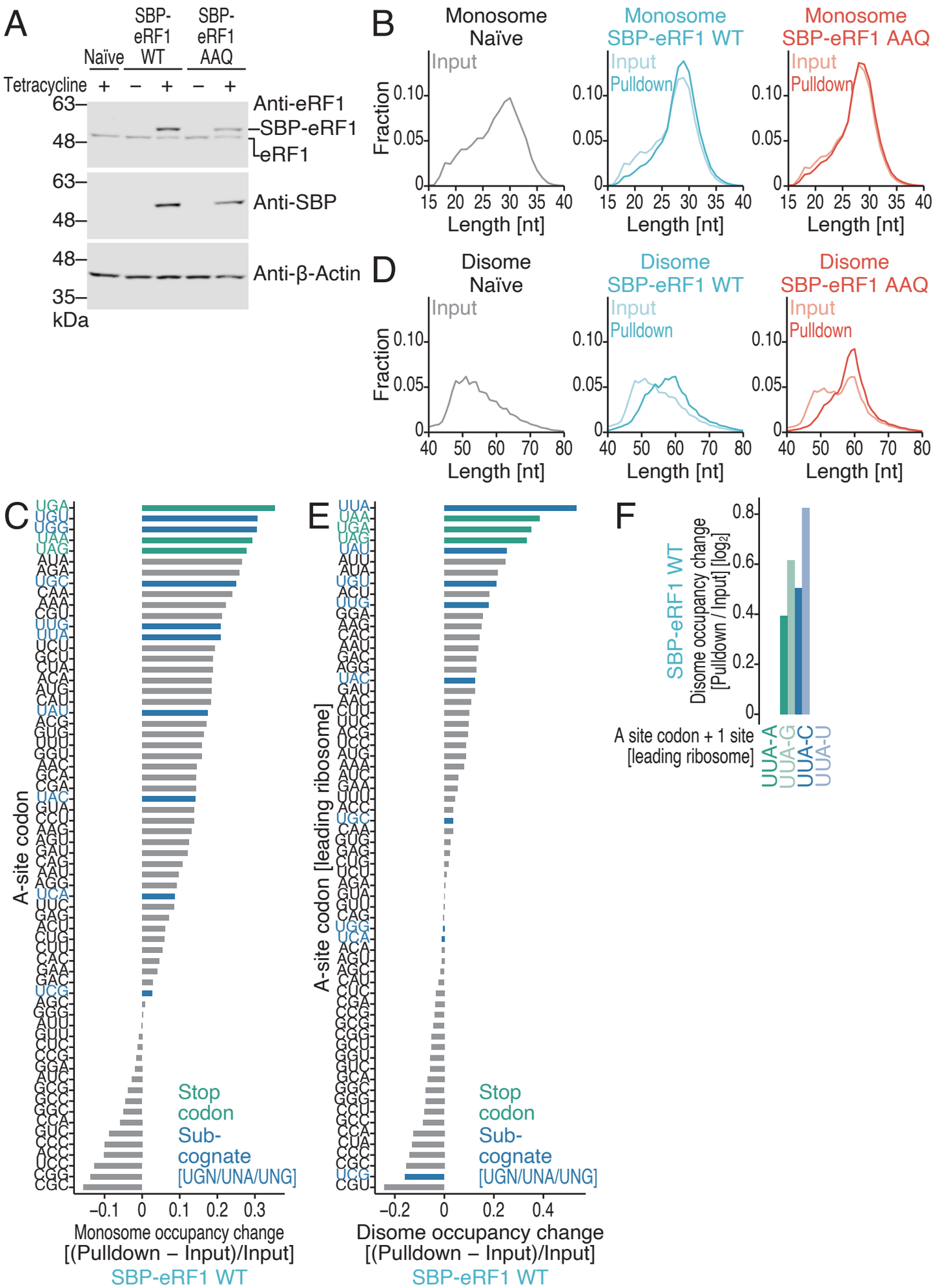

Figure S1 Han *et al.* (2024)

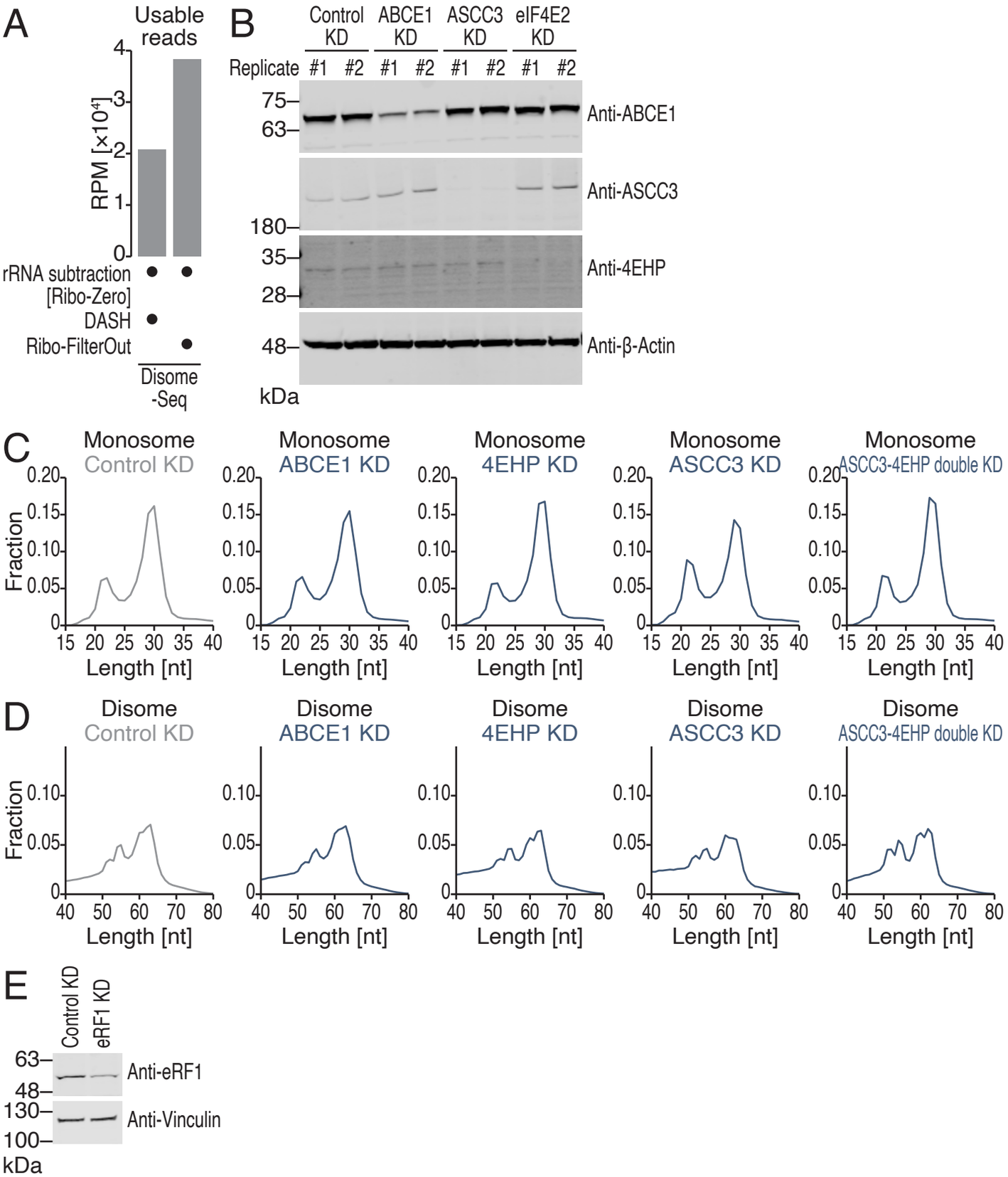

Figure S2 Han *et al.* (2024)

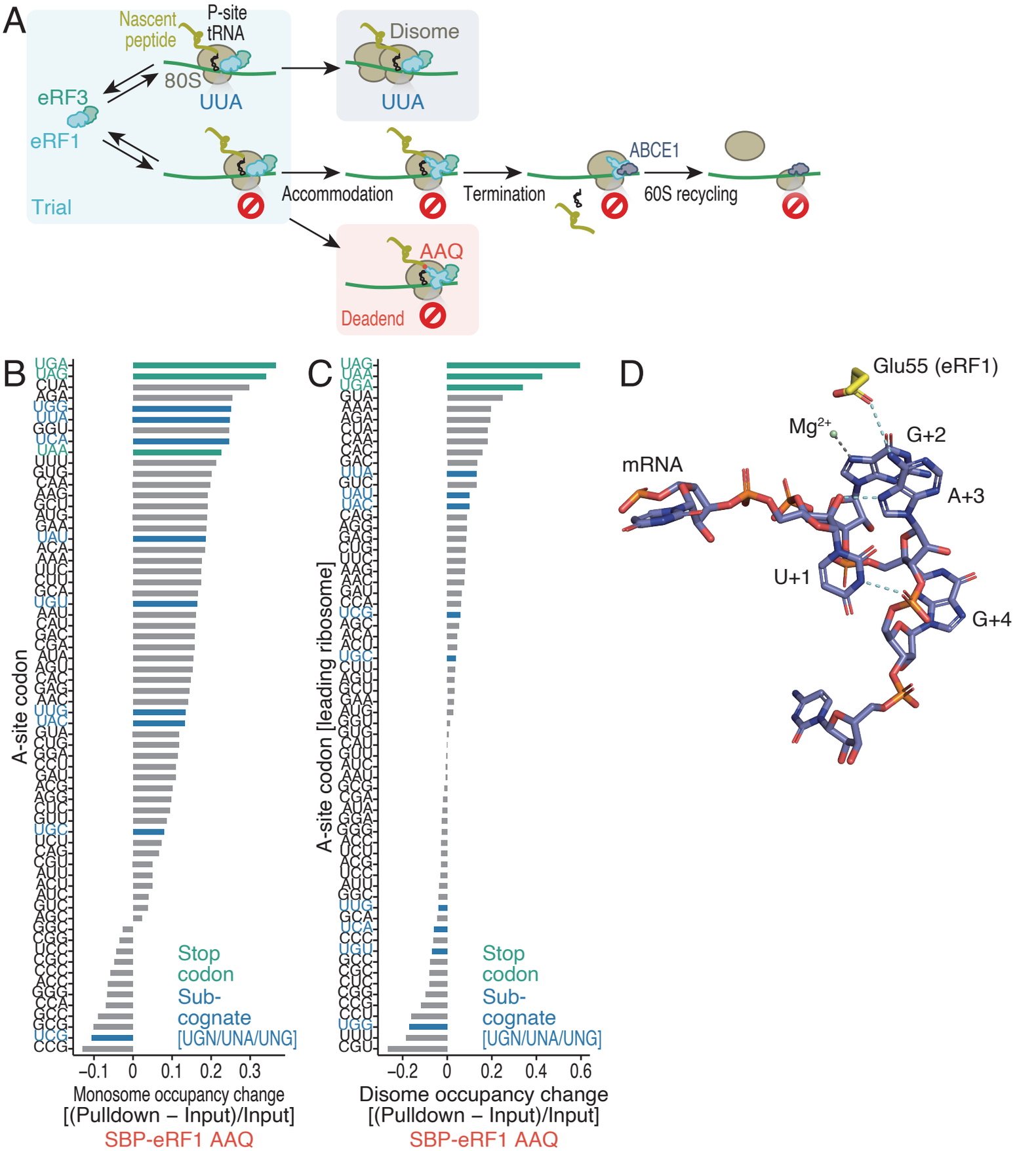

Figure S3 Han *et al.* (2024)

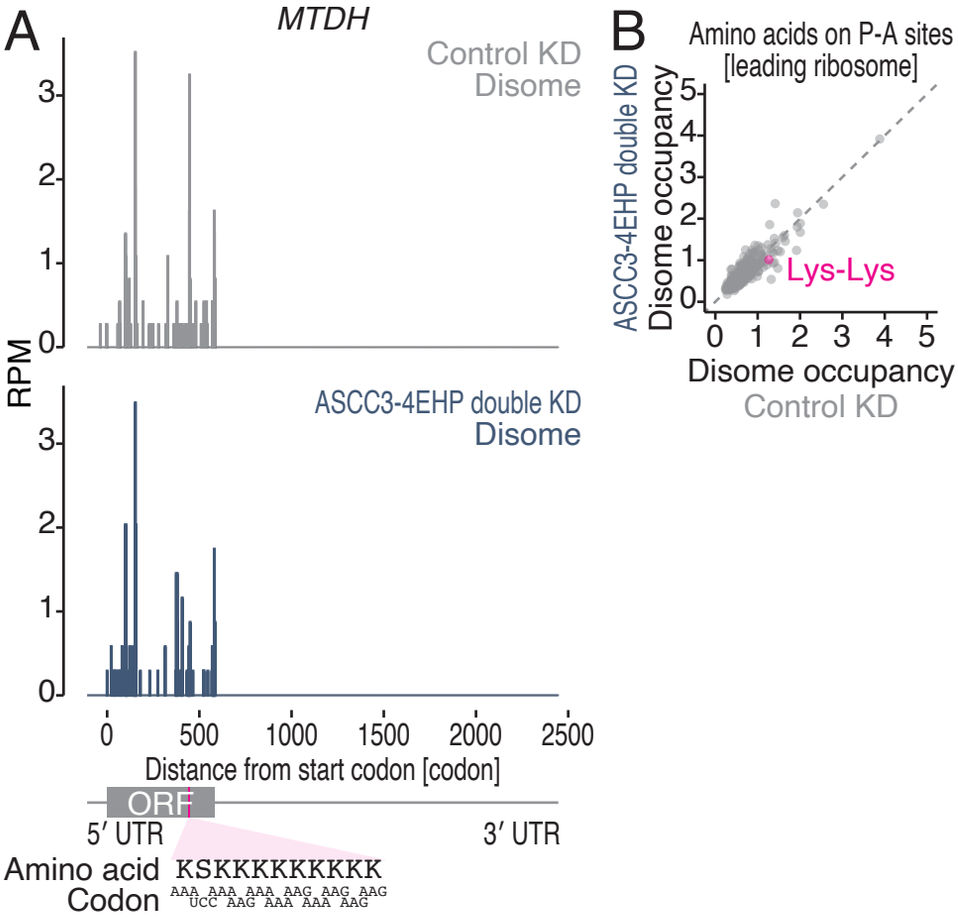

Figure S4 Han *et al*. (2024)